

# **SANDIA REPORT**

SAND2005-4648

Unlimited Release

Printed July 2005

## **The Equivalent Electrical Permittivity of Gas-Solid Mixtures at Intermediate Solid Volume Fractions**

Paul R. Tortora, Steven L. Ceccio, John R. Torczynski

Prepared by Paul Tortora  
Sandia National Laboratories  
Albuquerque, New Mexico 87185 and Livermore, California 94550

Sandia is a multiprogram laboratory operated by Sandia Corporation,  
a Lockheed Martin Company, for the United States Department of Energy's  
National Nuclear Security Administration under Contract DE-AC04-94AL85000.

Approved for public release; further dissemination unlimited.



**Sandia National Laboratories**

Issued by Sandia National Laboratories, operated for the United States Department of Energy by Sandia Corporation.

**NOTICE:** This report was prepared as an account of work sponsored by an agency of the United States Government. Neither the United States Government, nor any agency thereof, nor any of their employees, nor any of their contractors, subcontractors, or their employees, make any warranty, express or implied, or assume any legal liability or responsibility for the accuracy, completeness, or usefulness of any information, apparatus, product, or process disclosed, or represent that its use would not infringe privately owned rights. Reference herein to any specific commercial product, process, or service by trade name, trademark, manufacturer, or otherwise, does not necessarily constitute or imply its endorsement, recommendation, or favoring by the United States Government, any agency thereof, or any of their contractors or subcontractors. The views and opinions expressed herein do not necessarily state or reflect those of the United States Government, any agency thereof, or any of their contractors.

Printed in the United States of America. This report has been reproduced directly from the best available copy.

Available to DOE and DOE contractors from  
U.S. Department of Energy  
Office of Scientific and Technical Information  
P.O. Box 62  
Oak Ridge, TN 37831

Telephone: (865)576-8401  
Facsimile: (865)576-5728  
E-Mail: [reports@adonis.osti.gov](mailto:reports@adonis.osti.gov)  
Online ordering: <http://www.osti.gov/bridge>

Available to the public from  
U.S. Department of Commerce  
National Technical Information Service  
5285 Port Royal Rd  
Springfield, VA 22161

Telephone: (800)553-6847  
Facsimile: (703)605-6900  
E-Mail: [orders@ntis.fedworld.gov](mailto:orders@ntis.fedworld.gov)  
Online order: <http://www.ntis.gov/help/ordermethods.asp?loc=7-4-0#online>



SAND2005-4648  
Unlimited Release  
Printed July 2005

# The Equivalent Electrical Permittivity of Gas-Solid Mixtures at Intermediate Solid Volume Fractions

Paul R. Tortora, Steven L. Ceccio  
Thermal/Fluid Experimental Sciences

John R. Torczynski  
Microscale Science and Technology

Sandia National Laboratories  
P.O. Box 5800  
Albuquerque, New Mexico 87185-0834

## Abstract

Several mixture models are evaluated for their suitability in predicting the equivalent permittivity of dielectric particles in a dielectric medium for intermediate solid volume fractions (0.4 to 0.6). Predictions of the Maxwell, Rayleigh, Böttcher and Bruggeman models are compared to computational simulations of several arrangements of solid particles in a gas and to the experimentally determined permittivity of a static particle bed. The experiment uses spherical glass beads in air, so air and glass permittivity values (1 and 7, respectively) are used with all of the models and simulations. The experimental system used to measure the permittivity of the static particle bed and its calibration are described. The Rayleigh model is found to be suitable for predicting permittivity over the entire range of solid volume fractions (0-0.6).

## **Acknowledgments**

The authors wish to acknowledge the technical contributions of Steven M. Trujillo, Timothy J. O'Hern, and Kim A. Shollenberger. Thanks also to Sandia National Labs' skilled technologists: John Oelfke, Jeremy Barney, Ray Cote, Rocky Erven, Tom Grasser, Jaime Castañeda, and Rusty Spillers.

This work was funded by the US Department of Energy Office of Industrial Technologies under Field Work Proposal EEW-7924, Brian Valentine, program manager; and NSF award CTS-0074245, Michael W. Plesniak, program manager.

## Contents

1. Introduction .....	7
2. Mixture Models for Gas-solid Mixtures .....	9
3. Computational Simulations of Mixture Permittivity .....	13
4. Experimental Measurements .....	17
5. Results .....	21
6. Discussion .....	23
7. Conclusions .....	25
8. References.....	27

## Figures

Figure 1. Permittivity and voltage for computational simulations. ....	14
Figure 2. Distribution of permittivities obtained from 10,000 Monte Carlo simulations with solid volume fraction of 0.625. ....	15
Figure 3. EIT measurement circuit.....	17
Figure 4. Analytical models (curves) and computational and experimental results (symbols).....	22

## Nomenclature

### Roman:

$C_D$	flow domain capacitance
$C_E$	stray capacitance
$C_g$	capacitance of flow domain filled with air
$C_p$	capacitance of flow domain filled with particles
$C_S$	feedback capacitance
$R_f$	feedback resistance
$V_E$	carrier voltage
$V_{null}$	nulling voltage
$V_{out}$	output voltage of measurement circuit

### Greek:

$\epsilon_g$	dielectric permittivity of gas or air
$\epsilon_m$	dielectric permittivity of mixture of particles and gas
$\epsilon_p$	dielectric permittivity of particle bed
$\epsilon_s$	dielectric permittivity of particle material
$\phi, \phi_p$	volume fraction of particles
$\omega$	angular frequency

# 1. Introduction

Electrical impedance measurement techniques are used in a variety of industrial and experimental settings for the measurement of material distributions in two-phase flows. Electrical measurements with two or three electrodes can be performed to determine the bulk or local properties of a flow [1-9]. Alternatively, electrical-impedance tomography (EIT) uses multiple electrodes to spatially resolve material distributions [10-19]. In the latter case, a reconstruction algorithm [20-24] is necessary to determine the spatial impedance distribution based on the impedances measured by the electrodes. In both cases, a mixture model must be used to convert measured impedance to material distribution. Recent work in developing an EIT system [25] suggested that the accuracy of mixture models be investigated.

Some *a priori* knowledge of the two-phase flow is often used to select the mixture model. A straightforward example is a stratified flow, where the series impedance model may be appropriate. Another straightforward example is a flow containing a single or small number of spherical inclusions of one material within a second continuous material, in which case the exact solution for the electric field for spheres might be used. In most cases, however, the distribution of materials is not as well understood.

The present work involves gas-solid flows in a circulating fluidized bed (CFB) riser, to which a 16-electrode EIT system is applied [25]. The CFB contains dielectric particles – glass spheres or fluid catalytic cracking (FCC) catalyst – fluidized with air, so only the capacitive component of impedance is considered in this work. A variety of particle distributions are encountered in these experiments, ranging from dilute suspensions to packed beds (with solids fractions on the order of 0.6). For dilute suspensions, much work has been devoted to the calculation of the equivalent dielectric permittivity of particles dispersed in a continuous medium. The Maxwell model has been found to be accurate in many studies [1, 26, 27]. Although most other models are nearly identical to the Maxwell model (and therefore to each other) at very low solid volume fractions ( $<0.2$ ), most models differ significantly at higher solid volume fractions, for which the interactions of electric fields between particles become significant.

The equivalent permittivity of a randomly packed bed of particles is of interest in the current work because it is often used as a calibration condition for the EIT system. Relations for the permittivity of regular arrays of spheres [28-33] can be extended to the packing limit to estimate the permittivity of a packed bed. However, the permittivity of a packed bed is sensitive to the exact arrangement of particles, which varies strongly with the number of contact points between particles [29], which in turn varies among particle types for random packings.

The intermediate range of solid volume fractions (0.4-0.6) between dilute suspensions and packed beds (the “crossover region”) is the least well understood and is of primary interest in this work. Many researchers have attempted to model the equivalent mixture permittivity for disperse heterogeneous mixtures, with a recent review

provided by Torquato [34]. Many mixture models are formulated to account for dilute mixtures of monodisperse spheres with no contact (*e.g.*, the Maxwell model), and some of these models have been extended to larger solid volume fractions. Other models are formulated for lattices of spheres over a wide range of volume fractions [28-33]. Both analytical and numerical simulations have been performed for a wide variety of particle topologies. However, it is unclear whether or not a single relationship can be accurate over the entire range of solid volume fractions encountered in gas-solid flows (ranging from dilute to packed beds).

Numerous applications of bulk and local impedance measurements and EIT using a variety of mixture models appear in the literature [1-19], but few authors have reported systematic studies of the effect of their choice of mixture model on their results. Wiesendorf and Werther [9] discussed the influence of different mixture models on measurements from a capacitance probe, and McKeen and Pugsley [12] examined the influence of permittivity models on the reconstruction of cylindrical phantoms. The most systematic study of mixture models was performed reported by Louge and Opie [35]. They measured the permittivity of static suspensions of particles in petroleum jelly with various solid volume fractions, and also measured the permittivity of a packed bed of glass spheres in air.

The purpose of this work is to evaluate mixture models commonly used in the analysis of gas-solid impedance measurements – with emphasis on the accuracy of models in the crossover region – to determine whether or not a single model can be used over the full range of solid volume fractions (or conversely, where particular mixture models fail). Only dielectric materials are considered here (resistive materials and steady-state heat conduction generally have analogous models). Models assuming disperse mixtures of monodisperse spheres (the Maxwell, Böttcher, Rayleigh, and Bruggeman models) and assuming dense but non-contacting arrays of spheres (Rayleigh model) are examined. The transition between nearly touching and fully contacting spheres is also considered. Direct simulations of regular arrays of spheres and Monte Carlo simulations of random arrangements of cubes are performed. Experiments are performed to measure the solids volume fraction and impedance of a packed bed. The predictions of the various models are then compared to the measurements and simulations.

## 2. Mixture Models for Gas-solid Mixtures

The analytical models reviewed here include those most commonly used for the evaluation of gas-solid mixtures. Each model relates the gas permittivity  $\epsilon_g$ , the solid permittivity  $\epsilon_s$  and the particle volume fraction  $\phi$  to the equivalent mixture permittivity  $\epsilon_m$ . It is generally assumed that the particles are spherical and monodisperse. Scaife [27] and del Tin and Negrini [2] discuss mixture models that account for different particle shapes and size distributions.

The mixture impedance is bounded by the parallel and series mixture impedances, obtained by assuming that the materials distribution resembles parallel or series networks of capacitors:

$$\text{Parallel:} \quad \epsilon_m = \phi\epsilon_s + (1 - \phi)\epsilon_g \quad (1)$$

$$\text{Series:} \quad \frac{1}{\epsilon_m} = \frac{\phi}{\epsilon_s} + \frac{(1 - \phi)}{\epsilon_g} \quad (2)$$

Permittivity values outside of the envelope formed by the parallel and series models are not physically possible for the mixture. These models are not usually suitable for impedance measurements of multiphase flows; however, Warsito and Fan [13] used a weighted combination of the two.

The most commonly used model is that of Maxwell [1, 26, 27]:

$$\phi = \frac{(2 + \epsilon_s/\epsilon_g)(1 - \epsilon_m/\epsilon_g)}{(1 - \epsilon_s/\epsilon_g)(2 + \epsilon_m/\epsilon_g)} \quad (3)$$

It is derived for monodisperse spherical particles having negligible effects on the shapes of each other's electric fields. It is assumed that each particle is surrounded by a shell of the continuous phase which is in turn surrounded by a phase with the mixture conductivity. Those assumptions suggest that the model should be applied only to dilute, homogeneous distributions of monodisperse particles, but past investigations indicate that the model is robust: for example, it has been applied at high solid volume fractions for certain substances [36] and to polydisperse distributions of bubbles in water [11]. In general terms, the Maxwell model relates the mixture permittivity to the permittivity of a disperse phase (here  $\epsilon_s$ ), a continuous phase (here  $\epsilon_g$ ), and the volume fraction of the disperse phase (here  $\phi$ ). Equation 3 could be applied, for example, to an arrangement of inclusions of air in a continuous solid by interchanging  $\epsilon_g$  and  $\epsilon_s$  and replacing  $\phi$  with  $(1-\phi)$  to form a second relation between mixture permittivity and volume fraction. Other models can be rearranged in a similar fashion.

The Böttcher model [37] is an extension of the Maxwell model where the shell of continuous fluid is no longer assumed; rather, the particle is immersed in a fluid that has the mixture impedance:

$$\phi = \frac{(\epsilon_m - \epsilon_g)(\epsilon_s + 2\epsilon_m)}{(3\epsilon_m)(\epsilon_s - \epsilon_g)} \quad (4)$$

The Böttcher model is expected to be valid for higher solids fractions compared to the Maxwell model. Louge and Opie [35] found the Böttcher model to be suitable for predicting the permittivity of dispersions of fluid catalytic cracking (FCC) catalyst that had absorbed water by selecting the value of permittivity for FCC catalyst that best fit their data. Also, the Böttcher model is “symmetrical” in the sense that interchanging  $\epsilon_g$  and  $\epsilon_s$  and replacing  $\phi$  with  $(1-\phi)$  yields the same expression.

Rayleigh derived an expression for the equivalent permittivity of a cubical array of spheres; this expression has been adapted by a number of authors [37]. Here, a version derived by Meredith and Tobias [28] and recommended by Louge and Opie [35] for gas suspensions of spherical glass beads is considered:

$$\epsilon_m = \frac{\epsilon_g \left( \frac{2\epsilon_g + \epsilon_s}{\epsilon_g - \epsilon_s} - 2\phi + 0.409 \frac{6\epsilon_g + 3\epsilon_s}{4\epsilon_g + 3\epsilon_s} \phi^{7/3} - 2.133 \frac{3\epsilon_g - 3\epsilon_s}{4\epsilon_g + 3\epsilon_s} \phi^{10/3} \right)}{\left( \frac{2\epsilon_g + \epsilon_s}{\epsilon_g - \epsilon_s} + \phi + 0.409 \frac{6\epsilon_g + 3\epsilon_s}{4\epsilon_g + 3\epsilon_s} \phi^{7/3} - 0.906 \frac{3\epsilon_g - 3\epsilon_s}{4\epsilon_g + 3\epsilon_s} \phi^{10/3} \right)} \quad (5)$$

It is not possible to obtain an explicit expression for  $\phi$  from this relation.

Bruggeman extended Maxwell’s model to produce an expression for the equivalent permittivity of a random spatial distribution of randomly sized spheres [2] that is suitable for higher solid volume fractions [37]:

$$\phi = \left( \frac{\epsilon_s - \epsilon_m}{\epsilon_s - \epsilon_g} \right) \left( \frac{\epsilon_g}{\epsilon_m} \right)^{1/3} \quad (6)$$

In this case, although it is possible to obtain an explicit expression for  $\epsilon_m$  in terms of  $\phi$ , the form is extremely complicated.

As mentioned, a number of researchers have formulated mixture models for regular arrays of spheres [28-33]. These models are practically identical to the Rayleigh model up to a volume fraction of about 0.6. As the packing limit is approached, the models for simple-cubic, body-centered-cubic, and face-centered-cubic arrays diverge from the Rayleigh model due to various correction terms. Therefore, these models are not compared to the other models or simulations but are considered later in the discussion of results.

Additional methods of calculating the equivalent mixture permittivity include bounding methods and expansions, as comprehensively described by Torquato [34]. Because it is not usually possible to explicitly determine the properties of particle dispersions, bounding methods are applied to establish two curves between which the mixture permittivity is expected to fall (the parallel and series models are the simplest examples of such bounds). Expansions increase the accuracy of simple models by adding higher-order terms that account for additional particle interactions, as the models for lattices of spheres do [28-33].



### 3. Computational Simulations of Mixture Permittivity

Analytical solutions are not available for irregular packed beds of particles. The properties of an arbitrary matrix of solids can be directly computed, but the computational cost needed to resolve the electric field would be high. In the present work, the transition between disperse and packed particle arrangements is examined by computing the permittivity of regular arrays of spheres for increasing volume fraction up to and past the contacting limit. Monte Carlo simulations are also performed to calculate the mixture permittivity of random material distributions. Details of the simulation methods are presented below.

The commercial computational fluid dynamics code FIDAP<sup>TM</sup> (Fluent, Inc., Lebanon, NH) is used to perform computational simulations for comparison to the models and experimental data. The simulations are performed as heat-conduction problems because the equations governing electrostatics are of the same form mathematically as those governing steady heat conduction [38]: voltage corresponds to temperature, electrical permittivity corresponds to thermal conductivity, and electric current corresponds to heat flux. In all simulations, the gas and solid phases have permittivities of 1 and 7, respectively, which correspond to air and glass.

The first set of simulations involves simple cubic lattices of cubes and spheres of various sizes. The computational domain for these simulations is one octant of the simple cubic unit cell with a cube or sphere at the unit cell's center, the octant being a unit cube. Figure 1a shows examples of the permittivity and voltage contours in this cubical domain from one of the simulations for a sphere. The bottom and top of the cubical domain are set to constant voltages of 0 and 1, respectively, and symmetric boundary conditions are specified on the four sides. Adjacent spheres are allowed to overlap when their radii exceed the length of the domain. Rectangular grids are used for simplicity, with the permittivities of the two regions mapped onto the grid depending on radial position from the sphere's center. The grids are cubic except for the spherical simulations in which the spheres approached or touched the edge of the domain; in these cases grid elements are concentrated near the edges of the domain to ensure that the "cusp" formed by touching spheres is resolved adequately. The number of grid elements is equal to  $(8n)^3$  where  $n$  is a whole number; the grid is refined by increasing  $n$  until the difference between current flow for grids of  $(8n)^3$  and  $(8(n+1))^3$  elements is less than 1%. In most of the simulations,  $n$  is equal to 2 or 3. The currents flowing through the top and bottom of the domain, which should be equal by continuity, agree within 1% in all simulations. From the above choice of nondimensionalization, this current is equal to the mixture permittivity.

Simulations of a hexagonal lattice of spheres are also performed in the same manner. Figure 1b shows examples of the permittivity and voltage contours obtained from a simulation of the hex-close-packed arrangement. The domain is divided into three sections of identical geometry: the boundaries are drawn from the centerlines of the rectangular faces to the center of the triangular base, within each of which a Cartesian

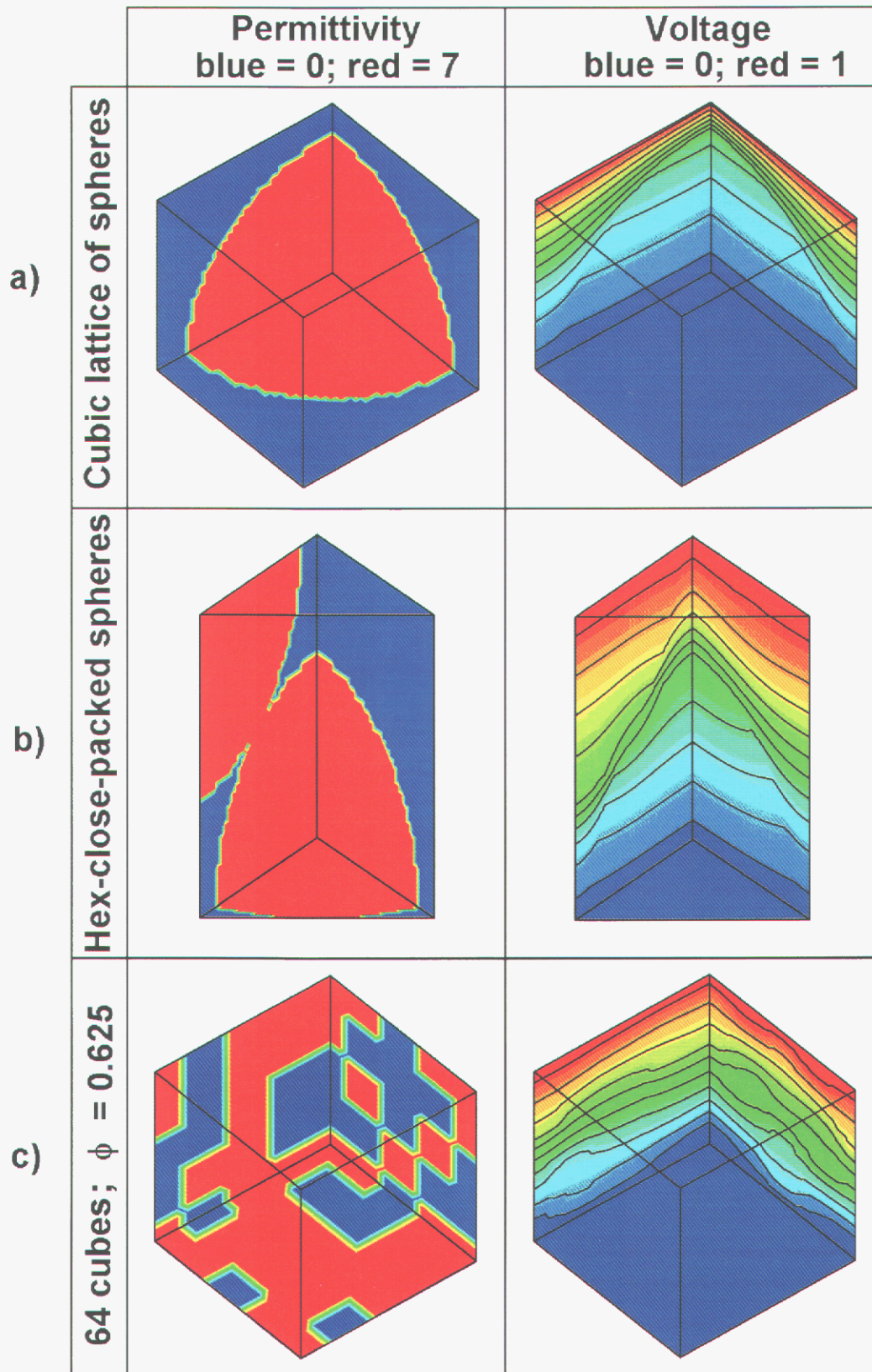
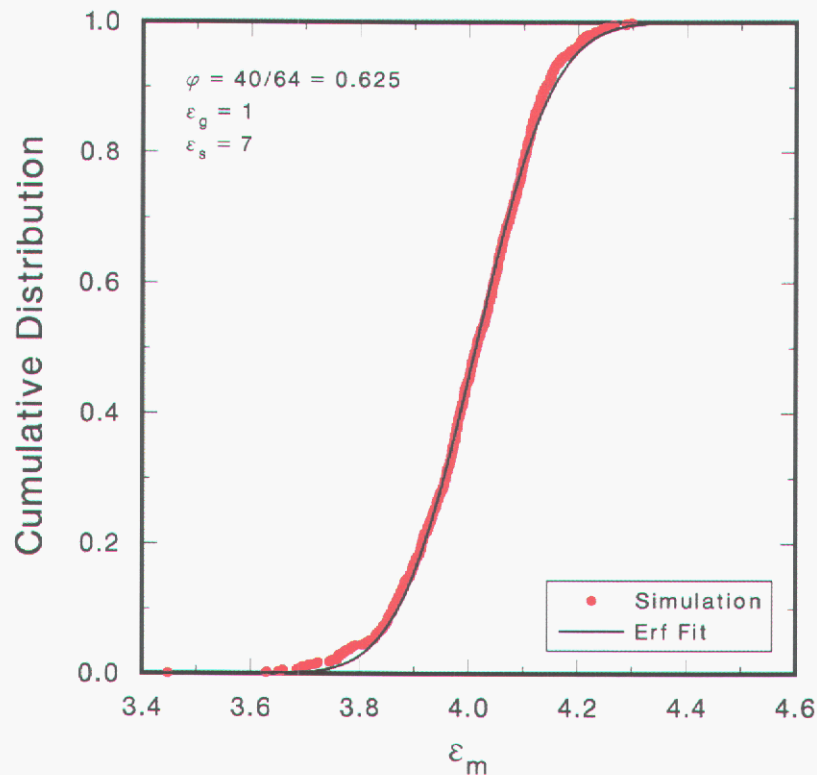


Figure 1. Permittivity and voltage for computational simulations.

grid is set up. The simulations are performed for various radii, and the spheres are allowed to overlap at high volume fractions as in the previous simulations.

The final set of simulations represents a more general approach to the arrangement of materials. A cubical domain is divided into 64 sub-cubes, within each of which the permittivity is set to either of two permittivity values in any combination. Figure 1c shows examples of the permittivity and voltage contours for one arrangement of 40 “solid” and 24 “gas” sub-cubes, corresponding to a solid volume fraction of 0.625. There are approximately  $2.5 \times 10^{17}$  possible arrangements of cubes for this volume fraction, and since the computational cost of simulating them all is prohibitive,  $10^4$  Monte Carlo simulations are performed. In each simulation, the numbers of solids and gas sub-cubes are fixed to yield the prescribed solid volume fraction, but the locations of these sub-cubes are assigned randomly. The cumulative distribution of permittivities obtained from these simulations is shown in Figure 2 and is well represented by an error function, so the probability distribution is approximately Gaussian. It is straightforward to obtain the mean and standard deviation of this distribution. Monte Carlo simulations are performed for several other solid volume fractions as well. Simulations for very high or low volume fractions (*i.e.*, only 1-3 cubes of either phase) do not require Monte Carlo methods because the total number of arrangements is relatively low (*e.g.*, only 41,664 arrangements of 3 cubes).



**Figure 2. Distribution of permittivities obtained from 10,000 Monte Carlo simulations with solid volume fraction of 0.625.**



## 4. Experimental Measurements

The mixture permittivity and volume fraction of a random-close-packed bed of glass beads were measured to provide an experimental comparison for the analytical models. The particles are glass beads (Potter Industries, Inc.), which are well characterized: they are solid spheres, have a known size distribution of 120-180 microns, and have a known dielectric permittivity of approximately 7. Since the materials under consideration are dielectric, only capacitive effects are considered: resistive effects are ignored. Bares [39] studied the surface conductivity of glass particles and noted that it becomes negligible at frequencies greater than 1 kHz (a frequency of 100 kHz is used for all applied voltages discussed below).

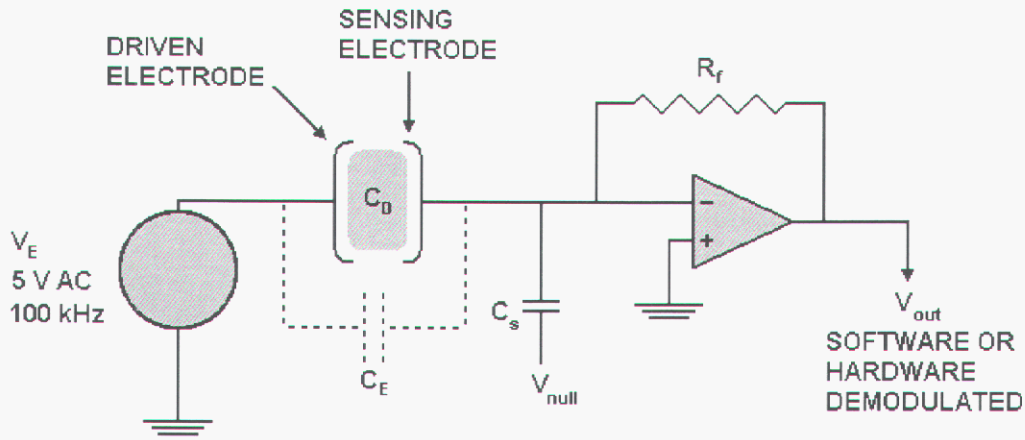


Figure 3. EIT measurement circuit.

Capacitances between electrode pairs are measured using the bridge circuit shown in Figure 3. Many variants of this measurement scheme are found in the literature [40-42]. The flow-domain capacitance  $C_D$  is related to the output voltage  $V_{out}$  by

$$V_E \omega (C_D + C_E) = V_{null} \omega C_S + \frac{V_{out}}{R_f} \quad (7)$$

where  $V_E$  is the carrier voltage,  $V_{null}$  is the nulling voltage,  $C_S$  is the feedback capacitance,  $C_E$  is the stray capacitance,  $R_f$  is the feedback resistance, and  $\omega = 2\pi f$  is the angular frequency. The stray capacitance includes the capacitance between the electrodes that does not lie within the flow region and the parasitic capacitances that exist between other parts of the circuit. This capacitance must be accounted for because it may be similar in magnitude to the flow-domain capacitance and can change (*e.g.*, with temperature changes or when the electrodes are moved to a different measurement location). Guard circuits and guard electrodes may be used to minimize the stray

capacitance, and a number of configurations appear throughout the literature. In the present experiments, a single ring of grounded shielding surrounds the electrodes (which, in turn, surround the experimental domain). This reduces stray capacitance somewhat, but further guarding could be installed in the future to further reduce it. The effect of reducing stray capacitance is to reduce noise in the measurement, but for the purposes of the experiments described here, the noise level was judged to be adequate.

The following calibration procedure is used to determine the stray capacitance. For each of two calibration conditions—an empty domain (*i.e.*, air) and a domain containing a bed of particles—the nulling voltage is adjusted so that the output voltage equals zero. This yields two forms of Equation 7, one in which the flow-domain capacitance  $C_D$  corresponds to the air value  $C_g$  and one in which  $C_D$  corresponds to the particle-bed value  $C_p$ . An additional equation relates the flow-domain capacitances of air and the particle bed to their respective permittivities  $\epsilon_g$  and  $\epsilon_p$  (not to be confused with the permittivity of the discrete solid material,  $\epsilon_s$ ) for an identical geometry:

$$\frac{C_p}{C_g} = \frac{\epsilon_p}{\epsilon_g} \quad (8)$$

where the permittivity of air is equal to unity and the particle-bed permittivity is assumed to have been previously determined. Solution of these three equations yields the unknown stray capacitance  $C_E$ . In these experiments,  $C_p$  ranged from tens to hundreds of femtofarads and  $C_E$  ranged from femtofarads to picofarads, depending on the angular separation between electrodes. The calibration is performed once per day and whenever the experimental equipment is physically moved (*i.e.*, the electrodes are moved to a different measurement location).

The permittivity of a particle bed is determined using a method similar to the procedure above. A third material—a transformer oil of known permittivity—is used, and since oil cannot be easily introduced into the multiphase flow experiment, this measurement is performed in an identical offline domain. The movement of the electrodes changes the stray capacitance, which is treated as an unknown. The offline domain is filled successively with air (of known permittivity  $\epsilon_g = 1$ ), a particle bed (of unknown permittivity  $\epsilon_p$ ), and the transformer oil (of known permittivity  $\epsilon_l > 1$ ). The nulling voltage is again adjusted such that the output voltage for each material is equal to zero, producing three forms of Equation 7. Two forms of Equation 8 are used to relate ratios of the capacitances and permittivities for air, the particle bed, and oil. Solving these five equations yields the desired particle-bed permittivity  $\epsilon_p$ . This determination need only be made once or, if a statistical sampling is required, only one set of measurements is needed. Note that the domain and electrode geometry in this offline calibration need not be identical to the online experiment: since the offline calibration measures a material property, any geometry should produce the same result. The offline calibration and the online experiment were performed in identical domains here for convenience.

Once the particle-bed permittivity and (online) stray capacitance are known, Equation 7 relates the measured output voltage to the unknown flow-domain capacitance in terms of known quantities. For flow measurements, the nulling voltage is used to balance the bridge when the flow domain is empty (*i.e.*, air-filled), and deflections of the bridge occur when particles are present (*i.e.*, during flow).

The final step in the technique is the use of a mixture model to relate the mixture permittivity  $\epsilon_m$  measured at a given flow state to the particle volume fraction  $\phi$ . A mixture model typically requires knowledge of the permittivity of the continuous-phase material,  $\epsilon_g$ , and the permittivity of the discrete-phase material,  $\epsilon_s$ . The quantity  $\epsilon_s$  may not be known *a priori* because many types of particles used in gas-solid processes are poorly characterized: they may be porous, and their composition may be proprietary. An example of such particles is FCC catalyst. In this situation, a mixture model can be used to infer the quantity  $\epsilon_s$  from the measured value of  $\epsilon_p$  at a known volume fraction of  $\phi_p$  (*e.g.*, random close-packed). If the quantity  $\epsilon_s$  is known, the measured values of  $\epsilon_p$  and  $\phi_p$  for the particle bed serve as a check on the accuracy of the mixture model.



## 5. Results

The models and simulations described above are investigated for permittivities of 1 (gas) and 7 (solid), which are the permittivities of air and glass, respectively. The simulations of simple cubic lattices of spheres and cubes are performed both for “ordinary” distributions, for which the spheres and cubes are identified as glass distributed in air, and for “inverse” distributions, for which the spheres and cubes are identified as air distributed in glass. The simulations of hexagonal lattices of spheres are performed only for ordinary distributions.

All of the analytical models mentioned previously—including the inverse versions of the Böttcher and Bruggeman models—along with the simulations results are plotted in Figure 4. The values for the Monte Carlo simulations are the means of the distributions obtained from those simulations (*e.g.*, the Monte Carlo value for the volume fraction of 0.625 is the mean of the distribution shown in Figure 2). The experimental value for a bed of glass beads—measured using the calibration procedure discussed previously—also appears on the plots. The volume and weight of a bed of particles were measured to obtain its density, which was divided by the density of solid glass to obtain the particle-bed solid volume fraction. The uncertainty in the values obtained from the computational simulations is approximately 2%, based on the previously discussed differences between simulation results with successive grid refinements and the differences between computed current flows through the top and bottom of the simulation domains. The uncertainty in the experimental value is also approximately 2%.

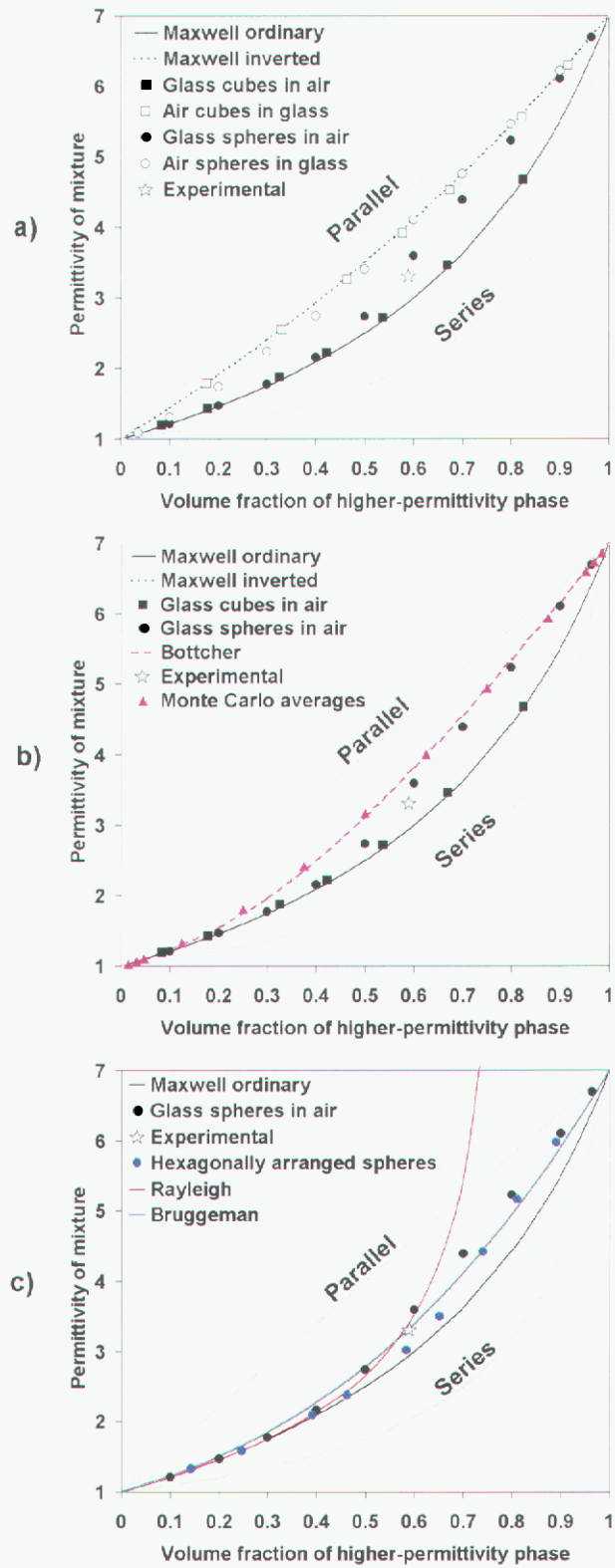


Figure 4. Analytical models (curves) and computational and experimental results (symbols).

## 6. Discussion

The parallel and series models are too extreme to predict the equivalent permittivity of particle distributions, as mentioned previously, and Figure 4 shows that those models do not agree with the other models, the simulations, or the experimental value. These models do, however, establish an envelope within which all of the other models, the simulations, and the experimental value fall, with the exception of the Rayleigh model, which was not derived for volume fractions exceeding that of a simple cubic close-packing of spheres. (The volume fractions of simple cubic and hexagonal lattices of close-packed spheres are  $\pi/6 \approx 0.52$  and  $2^{1/2}\pi/6 \approx 0.74$ , respectively.)

The contrast between the Maxwell models and the simulations shown in Figure 4a is instructive. The simulations of simple cubic lattices of glass cubes surrounded by air and the Maxwell model agree, as do the inverse versions. The simulations of simple cubic lattices of glass spheres surrounded by air agree with the Maxwell model for low volume fractions, but trend towards the inverse Maxwell model as the spheres become close, and overlap and agree with the inverse Maxwell model at the highest volume fractions. This makes sense: as the volume fraction is increased, the spheres overlap and enclose the air between them so that inclusions of air (somewhat diamond-shaped) are surrounded by glass. A similar but weaker trend is observed for the simulations of simple cubic lattices of spheres of air surrounded by glass.

The simulations for hexagonal lattices of spheres shown in Figure 4c also agree with the Maxwell model at low volume fractions and trend towards the inverse model as the volume fraction is increased. They depart from the Maxwell model at a higher volume fraction than the simulations of simple cubic lattices of spheres do because spheres in a hexagonal lattice touch at a higher volume fraction than spheres in a simple cubic lattice. These trends—along with the agreement of simple cubic lattices of cubes with the Maxwell model at all volume fractions—indicate that the Maxwell model is accurate as long as the phase identified as “continuous” is interconnected. The fact that the spherical simulations trend away from the Maxwell model at volume fractions slightly lower than those at which the spheres touch has two possible explanations: the model may not be accurate when interconnections in the continuous phase are very thin (like the spaces between nearly-touching spheres), or the computational grid is too coarse to capture the interconnections when the spheres are very close. Based on the mesh-sensitivity studies, the former explanation is preferred.

The Maxwell and Rayleigh models and the simulations of glass cubes and spheres surrounded by air all agree in the low-volume-fraction range of 0-0.4. The fact that the simulations all agree despite different shapes and arrangements of particles suggests that the Maxwell and Rayleigh models are robust in this range. These models are not expected to be accurate for multiphase flows with high solid volume fractions (*e.g.*, bubbling bed). This could lead to errors in measurements of gas-solid flows in the fast-fluidization regime, characterized by dense particle clusters at the walls of a riser [43]. Little is known about the structure of clusters, but the particles are fluidized, so it seems unlikely for their solid volume fractions to approach that of a packed bed. Therefore,

although the error due to clustering is expected to be small, it has not been quantified and should be explored in future work.

The Rayleigh model agrees best with the simulations for intermediate volume fractions (0.4-0.6), and correctly predicts the equivalent permittivity of a bed of glass beads (therefore correctly predicting the known permittivity of solid glass). This appears to be fortuitous, as simulations of simple cubic and hexagonal arrays of spheres disagree with the experimental value. Analytical expressions for simple-cubic, body-centered-cubic, and face-centered-cubic arrays of spheres also diverge from the Rayleigh model near the packing limit, as mentioned earlier [28-33]. This is explained by Batchelor and O'Brien [29] in their discussion of the effects of the number of contact points between spheres on the equivalent permittivity of randomly packed beds. Therefore, the permittivity of randomly packed beds of other types of particles should be considered on a case-to-case basis.

The Böttcher model does not appear suitable for this experiment, but it does match the average values of the Monte Carlo simulations closely as shown in Figure 4b. Recall that each Monte Carlo value in the figure represents the average of a set of simulations at the prescribed solid volume fraction. These average values coincide with the most homogeneous distributions of the 64 sub-cubes used in the simulations. This is also consistent with the model's "symmetry." Therefore, the Böttcher model appears well suited for predicting the permittivity of very homogeneous material distributions.

## 7. Conclusions

Several models relating the solid volume fraction and the equivalent mixture permittivity of distributions of dielectric particles in a gas are presented and compared to computational simulations. These models are evaluated for their suitability for calculating the equivalent mixture permittivity of distributions of the glass beads present in a multiphase flow experiment, especially in the intermediate volume fraction range of 0.4-0.6. The models and simulations all agree closely in the dilute solid volume fraction range of 0-0.4. The Rayleigh model is accurate over the intermediate range of solid volume fractions as well and appears most suitable for use with impedance measurements. The Rayleigh model also accurately predicts the permittivity of a particle bed, but this result is not expected to extend to random packings of other types of particles. Therefore, EIT studies of dense particle arrangements should be approached carefully.

The agreement between spherical models at low solid volume fractions (0-0.4) shows that the equivalent permittivity is relatively insensitive to the configuration and anisotropy of the materials. Also, comparing the simulations of spheres to the ordinary and inverted Maxwell models is instructive, showing that the simulations follow the ordinary model until the materials “swap roles” (the dispersed phase becomes the continuous phase, and vice versa) and follow the inverted model. It is also noted that all of the computational and experimental results fall between the ordinary and inverted Maxwell curves, and most realistic particle distributions are likely bounded by those models. Finally, the agreement between the Böttcher model and the mean permittivities of the Monte Carlo simulations suggests that the Böttcher model is well suited for predicting the permittivity of very homogeneous material distributions. This is also consistent with the fact that the Böttcher model is symmetrical (i.e., the model produces the same result regardless of how the phases are identified). Over 100,000 three-dimensional FEM calculations were performed to obtain these results.



## 8. References

- [1] Ceccio S.L. and George D.L. 1996 A review of electrical impedance techniques for the measurement of multiphase flows *J. Fluids Eng.* **118** 391-399
- [2] del Tin G. and Negrini A. 1980 Development of the electrical impedance probes for void fraction measurements in air-water flow *Multiphase Transport: Fundamentals, Reactor Safety, Applications* ed T. N. Veziroglu (Washington: Hemisphere) pp 2709-2730
- [3] Acree Riley C. and Louge M. 1989 Quantitative capacitive measurements of voidage in gas-solid flows *Part. Sci. Technol.* **7** 51-59
- [4] Das R.K. and Pattanayak S. 1993 Electrical impedance method for flow regime identification in vertical upward gas-liquid two-phase flow *Meas. Sci. Technol.* **4** 1457-1463
- [5] Das R. and Pattanayak S. 1994 Measurement of void fraction in different flow regimes of a vertical gas-liquid flow through narrow tubes *Meas. Sci. Technol.* **5** 1538-1545
- [6] Hage B. and Wether J. 1997 The guarded capacitance probe – a tool for the measurement of solids flow patterns in laboratory and industrial fluidized bed combustors *Powd. Technol.* **93** 235-245
- [7] Louge M., Lischer D.J. and Chang H. 1990 Measurements of voidage near the wall of a circulating fluidized bed riser *Powd. Tech.* **62** 269-276
- [8] Louge M., Tuccio M., Lander E. and Connors P. 1996 Capacitance measurements of the volume fraction and velocity of dielectric solids near a grounded wall *Rev. Sci. Instr.* **67** 1896-1877
- [9] Wiesendorf V. and Werther J. 2000 Capacitance probes for solids volume concentration and velocity measurements in industrial fluidized bed reactors *Powd. Tech.* **110** 143-157
- [10] Dyakowski T., Jeanmeure L.F.C. and Jaworski A.J. 2000 Applications of electrical tomography for gas-solids and liquid-solids flows – a review *Powd Tech.* **112** 174-192
- [11] George D.L., Torczynski J.R., Shollenberger K.A., O'Hern T.J. and Ceccio S.L. 2000 Validation of electrical-impedance tomography for measurements of material distribution in two-phase flows *Int. J. Multiph. Flow* **26** 549-581
- [12] McKeen T.R. and Pugsley T.S. 2002 The influence of permittivity models on phantom images obtained from electrical capacitance tomography *Meas. Sci. Technol.* **13** 1822-1830

- [13] Warsito W. and Fan L.-S. 2003 ECT Imaging of three-phase fluidized bed based on three-phase capacitance model *Chem. Eng. Sci.* **58** 823-832
- [14] Gamio J.C. 2002 A comparative analysis of single- and multiple-electrode excitation methods in electrical capacitance tomography *Meas. Sci. Technol.* **13** 1799-1809
- [15] Jaworski A.J. and Dyakowski T. 2001 Application of electrical capacitance tomography for measurement of gas-solid flow characteristics in a pneumatic conveying system *Meas. Sci. Technol.* **12** 1109-1119
- [16] Mohamad-Saleh J. and Hoyle B.S. 2002 Determination of multi-component flow process parameters based on electrical capacitance tomography data using artificial neural networks *Meas. Sci. Technol.* **13** 1815-1821
- [17] Mosorov V., Sankowski D., Mazurkiewicz L. and Dyakowski T. 2002 The 'best-correlated pixels' method for solid mass flow measurements using electrical capacitance tomography *Meas. Sci. Technol.* **13** 1810-1814
- [18] Wang M., Yin W. and Holliday N. 2002 A highly adaptive electrical impedance sensing system for flow measurement *Meas. Sci. Technol.* **13** 1884-1889
- [19] Yang W.Q. 1996 Calibration of capacitance tomography systems: a new method for setting system measurement range *Meas. Sci. Technol.* **7** 863-867
- [20] Fang W. 2004 A nonlinear image reconstruction algorithm for electrical capacitance tomography *Meas. Sci. Technol.* **15** 2124-2132
- [21] Loser T., Wajman R. and Mewes D. 2001 Electrical capacitance tomography: image reconstruction along electrical field lines *Meas. Sci. Technol.* **12** 1083-1091
- [22] Isaksen O. 1996 A review of reconstruction techniques for capacitance tomography *Meas. Sci. Technol.* **7** 325-337
- [23] Warsito W. and Fan L.-S. 2001 Neural network based multi-criterion optimization image reconstruction technique for imaging two- and three-phase flow systems using electrical capacitance tomography *Meas. Sci. Technol.* **12** 2198-2210
- [24] Yang W.Q. and Peng L. 2003 Image reconstruction algorithms for electrical capacitance tomography *Meas. Sci. Technol.* **14** R1-R13
- [25] Tortora P.R., Ceccio S.L., Trujillo S.M., O'Hern T.J. and Shollenberger K.A. Capacitance measurements of solid concentration in gas-solid flows *Powd. Technol.* **148** 92-101
- [26] Louge M. and Opie M. 1990 Measurements of the effective dielectric permittivity of suspensions *Powd. Technol.* **62** 85-94
- [27] Scaife B.K.P. 1989 *Principles of Dielectrics* (New York: Oxford)

- [28] Meredith R.E. and Tobias C.W. 1960 Resistance to potential flow through a cubical array of spheres *J. Appl. Phys.* **31** 1270-1273
- [29] Batchelor G.K. and O'Brien R.W. 1977 Thermal or electrical conduction through granular material *Proc. R. Soc. Lond. A* **355** 313-333
- [30] McPhedran R.C. and McKenzie D.R. 1978 The conductivity of lattices of spheres I. The simple cubic lattice *Proc. R. Soc. Lond. A* **359** 45-63
- [31] McKenzie D.R., McPhedran R.C. and Derrick G.H. 1978 The conductivity of lattices of spheres II. The body centred and face centred cubic lattices *Proc. R. Soc. Lond. A* **362** 211-232
- [32] Bergman D.J. 1979 The dielectric constant of a simple cubic array of identical spheres *J. Phys. C: Solid State Phys.* **12** 4947-4960
- [33] Sangani A.S. and Acrivos A. 1983 The effective conductivity of a periodic array of spheres *Proc. R. Soc. Lond. A* **386** 263-275
- [34] Torquato, S. 2002 *Random Heterogeneous Materials* (New York: Springer-Verlag)
- [35] Louge M. and Opie M. 1990 Measurements of the effective dielectric permittivity of suspensions *Powd. Tech.* **62** 85-94
- [36] Turner J.C.R. 1976 The electrical conductance of liquid-fluidized beds of spheres *Chem. Eng. Sci.* **31** 487-492
- [37] van Beek L.K.H. 1967 Dielectric behaviour of heterogeneous systems *Progress in Dielectrics v. 7* ed. J.B. Birks (Cleveland: CRC) pp 69-114
- [38] Lienhard, J.H. IV and Lienhard J.H. V 2001 *A Heat Transfer Textbook* (Cambridge: Phlogiston)
- [39] Bares J. 1988 Electrical conductivity of packed particle beds *IEEE Trans. Ind. Appl.* **24** 1050-1056
- [40] Huang S.M., Xie C.G., Thorn R., Snowden D. and Beck M.S. 1992 Design of sensor electronics for electrical capacitance tomography *IEEE Proc. G* **139** 83-88
- [41] Williams P. and York T. 1999 Evaluation of integrated electrodes for electrical capacitance tomography *1st World Congress on Industrial Process Tomography* Buxton, Greater Manchester Apr. 14-17 1999
- [42] Georgakopoulos D., Waterfall R.C. and Yang W.Q. 2001 Towards the development of a multiple-frequency ECT system *2nd World Congress on Industrial Process Tomography* Hannover, Germany Aug. 29-31 2001

[43] Grace J.R., Avidan A.A. and Knowlton T.M. 1997 Circulating Fluidized Beds  
(Blackie: London)

## Distribution:

1	MS0384	Ratzel, A. C.	Org. 9100
1	MS0825	Herminal, W. L.	Org. 9110
1	MS0834	Johannes, J. E.	Org. 9112
1	MS1310	Kempka, S. N.	Org. 9113
1	MS0834	Lash, J. S.	Org. 9114
1	MS0825	Hassan, B.	Org. 9115
1	MS0836	Hertel, E. S.	Org. 9116
1	MS0836	Griffith, R. O.	Org. 9117
1	MS0834	Cooper, M. A.	Org. 9112
2	MS0834	O'Hern, T. J.	Org. 9112
2	MS0834	Tortora, P. R.	Org. 9112
2	MS0834	Trujillo, S. M.	Org. 9112
4	MS0826	Torczynski, J. R.	Org. 9113
1	MS9018	Central Technical Files	8945-1
2	MS0899	Technical Library	9616

## External:

1	Professor S. L. Ceccio Mechanical Engineering 2011 Auto Lab University of Michigan Ann Arbor, MI 48109-2121
1	Dr. D. L. George Southwest Research Institute 6220 Culebra Rd. San Antonio, TX 78238-5166
1	Professor W. W. Schultz Mechanical Engineering 2027 Auto Lab University of Michigan Ann Arbor, MI 48109-2121
1	Associate Professor K. A. Shollenberger Mechanical Engineering Department California Polytechnic State University San Luis Obispo, CA 93407